Quaternary Science Reviews 28 (2009) 433–448

Contents lists available at ScienceDirect

Quaternary Science Reviews

journal homepage: www.elsevier.com/locate/quascirev

# Development and mass movement processes of the north-eastern Storegga Slide

Aaron Micallef*, Douglas G. Masson, Christian Berndt, Dorrik A.V. Stow

*National Oceanography Centre, University of Southampton, European Way, Southampton, SO14 3ZH, UK*

ARTICLE INFO

*Article history:*
Received 24 February 2008
Received in revised form
23 September 2008
Accepted 25 September 2008

ABSTRACT

The Storegga Slide, which occurred ~8100 years ago, is one of the world's largest and best studied exposed submarine landslides. In this study we use novel geomorphometric techniques to constrain the submarine mass movements that have shaped the north-eastern Storegga Slide, understand the link between different forms of failure, and propose a revised development model for this region. According to this model, the north-eastern part of the Storegga Slide has developed in four major events. The first event (event 1) was triggered in water depths of 1500–2000 m. In this event, the surface sediments were removed by debris flows and turbidity currents, and deposited in the Norwegian Sea Basin. Loading of the seabed by sediments mobilised by the debris flows and turbidity currents resulted in the development of an evacuation structure. Loss of support associated with this evacuation structure, reactivation of old headwalls and seismic loading activated spreading in the failure surface of event 1 up to the main headwall (event 2). In some areas, spreading blocks have undergone high displacement and remoulding. Parts of the spreading morphology and the underlying sediment have been deformed or removed by numerous debris flows and turbidity currents (event 3). We suggest that the higher displacement and remoulding of the spreading blocks, and their removal by debris flows and turbidity currents, was influenced by increased pore pressures, possibly due to gas hydrate dissolution/dissociation or by lateral variability in the deposition of contourite drifts in palaoeslide scars. The fourth event entailed a large, blocky debris flow that caused localised compression and transpressive shearing in the southern part of the spreading area.



## 1. Introduction

The Storegga Slide is a giant submarine landslide that occurred on the mid-Norwegian margin, about 120 km off the western coast of Norway (Bugge, 1983; Fig. 1). The Storegga region has a long history of slope instability related to the cyclic nature of sedimentation during glacial to interglacial climatic oscillations (Solheim et al., 2005). Glacigenic debris flow deposits, proximal glacial marine sediments and till, deposited during glacial periods, are interlayered with contouritic, hemipelagic and glacial marine sediments, deposited during interglacial periods (Berg et al., 2005). This stratigraphic framework, combined with the development of high pore water pressures due to rapid deposition of the glacial sediments, have preconditioned the Storegga region to fail during interglacial periods in the last 0.5 Ma (Bryn et al., 2003; Berg et al., 2005). Post-glacial isostatic rebound resulted in increased seismicity, providing possible triggers for submarine slope failure (Bungum et al., 2005).

The discovery of the Ormen Lange gas field close to the main headwall of the Storegga Slide has renewed the interest of industry and academia in this submarine landslide during the past decade (Fig. 1). Today a very large database of geophysical data and geotechnical boreholes is available for the Storegga Slide. The overall development of the Storegga Slide has been investigated and summarised in three key papers (Haflidason et al., 2004; Bryn et al., 2005a; Haflidason et al., 2005). These studies were based on a thorough visual interpretation of the bathymetric data from the slide scar, complemented by the analyses of sidescan sonar imagery and seismic data.

Geomorphometry, a field of research that was developed within the broader discipline of geomorphology, involves the quantitative characterisation of terrain surfaces. In geomorphometry, mathematical and statistical processing techniques are employed to quantify aspects of the land surface and facilitate the mapping, modelling and understanding of the formative geological processes. Geomorphometric techniques avoid problems of subjectivity and have been shown to be rapid, accurate and reproducible (Evans, 1990; Drăgut and Blaschke, 2006). Recent studies demonstrate that the geological interpretation of bathymetric data is improved if geomorphometric techniques are used (Mitchell and Clarke, 1994; Micallef et al., 2007b).

* Corresponding author. Tel.: +44 23 80 596563; fax: +44 2380 596554.
*E-mail addresses:* amicall@noc.soton.ac.uk, micallefaaron@hotmail.com (A. Micallef).

0277-3791/$ – see front matter © 2008 Elsevier Ltd. All rights reserved.
doi:10.1016/j.quascirev.2008.09.026

In this paper we use a number of geomorphometric techniques to characterise the morphology of the north-eastern Storegga Slide and improve the development model put forward by Haflidason et al. (2004). By investigating a major slide event in unprecedented detail and within an extremely well-known geological framework, this study provides a more profound understanding of the formative submarine mass movements, the associated geological processes and controls, and the way in which submarine mass movements are interrelated. Comprehension of the causes and development of submarine mass movements within the Storegga Slide also provides insight into the geological processes responsible for other submarine landslides located along the Norwegian margin, as the geological setting in which they occur is very similar (Rise et al., 2005). Submarine mass movements are a potential geohazard to hydrocarbon production, in particular the transport structures located on the Storegga Slide seabed. Improved modelling of submarine landslides is thus essential for assessing the risk associated with these geohazards. The highest resolution and density of acoustic data are found in the Ormen Lange region, and most of the studies of the Storegga Slide have been based on data from this part of the slide scar (e.g. De Blasio et al., 2004; Gauer et al., 2005; Kvalstad et al., 2005). Much less attention has been given to mass movements in the north-eastern Storegga Slide, which will be the focus of multiple proposed IODP drill sites in the near future (Brown et al., 2006). We therefore focus our geomorphometric analyses on data from the north-eastern Storegga Slide.

The objectives of this paper are: (a) to map the submarine mass movements that have shaped the north-eastern Storegga Slide; (b) to identify the geological factors and processes responsible for these mass movements; and (c) to propose a revised development model for the north-eastern Storegga Slide.

The nomenclature that will be used in this paper is the following: (i) zone: an area of seabed with specific and uniform morphological characteristics; (ii) lobe: individual or group of mass movements in the development model of the Storegga Slide proposed by Haflidason et al. (2004); and (iii) event: individual or group of mass movements as identified by ourselves in the revised development model of the Storegga Slide.

## 2. Regional setting

### 2.1. The Storegga Slide: morphology and slide development

The Storegga Slide, dated to ca 8100 ± 250 cal yr BP (Haflidason et al., 2005), influenced a total area of 95,000 km$^2$. During this event, it is estimated that 3200 km$^3$ of sediment was mobilised, with a maximum run-out distance of ~800 km. Almost 30% of the Storegga Slide area is comprised of the slide scar, which is characterised by an amphitheatre-shaped bathymetric depression located downslope of the shelf break (Fig. 1). The main headwall of the slide is 320 km long; it is up to 160 m high and has slope gradients of up to 45° (Micallef et al., 2007b). The slide scar surface has a mean slope gradient of 0.7°.

A detailed study of the surface sediment ages, seabed morphology and internal architecture of the slide scar by Haflidason et al. (2004) and Haflidason et al. (2005) revealed that the Storegga Slide was a quasi-simultaneous, multi-phase retrogressive event. This event mobilised five main partially superimposed slide lobes (lobes 1–5, in stratigraphical order), which represent more than 99% of the total volume of sediment involved in the Storegga Slide (Fig. 1). Lobe 1 covered the northern half of the Storegga Slide scar. During its development, sediment was removed in the form of debris flows and turbidity currents, and transported into the Norwegian Sea Basin. Lobe 1 extended upslope, on average, to within 20 km of the main Storegga Slide headwall. In lobe 2, detachment followed a failure plane deeper than that of lobe 1. Lobe 2 consisted of debris flows that mobilised large blocks of consolidated sediment. During the development of lobe 2, the mobilisation of sediment from the Ormen Lange region is thought to have been responsible for the generation of a tsunami and the formation of compression zones in the western part of the slide scar (Fig. 1) (Bryn et al., 2005a). Lobe 3 occurred along the same failure surface as the first lobe. It failed in the same way as lobe 1, although it affected a somewhat smaller area and extended further upslope to the main headwall. Lobe 4 was released after lobe 3 and is characterised by sub-parallel, partly disintegrated blocky structures located in the southern part of the slide scar. Lobe 5 was the last major debris flow and it influenced sediments inside and downslope of the Ormen Lange region. In addition to these five lobes there are more than 60 smaller individual slide events identified within lobes 2, 4 and 5. The dimensions of the lobes range from an area of 38,740 km$^2$ and a run-out distance of 450 km for first major phase, to an area of 0.3 km$^2$ for minor slides located close to the main headwall (De Blasio et al., 2003; Haflidason et al., 2004).

### 2.2. Study area: physiography and stratigraphy

The study area is the north-eastern Storegga Slide scar, north of the Ormen Lange gas field (Figs. 1, 2a). It is bound by the northern sidewall and Vøring Plateau to the north, the main Storegga headwall to the east, the S and R headwalls to the west, and the O headwall to the south. The area of seafloor under consideration is ~6850 km$^2$. The average slope gradient is 2.14°; the upslope part of the study area is steeper, but the slope becomes gentler with increasing depth (Figs. 2b, 3b). The depth of the seabed increases gently from ~250 m at the main headwall to 1550 m at the S headwall (Fig. 2b). Overall, the study area has the shape of a basin (Figs. 2b, 3a).

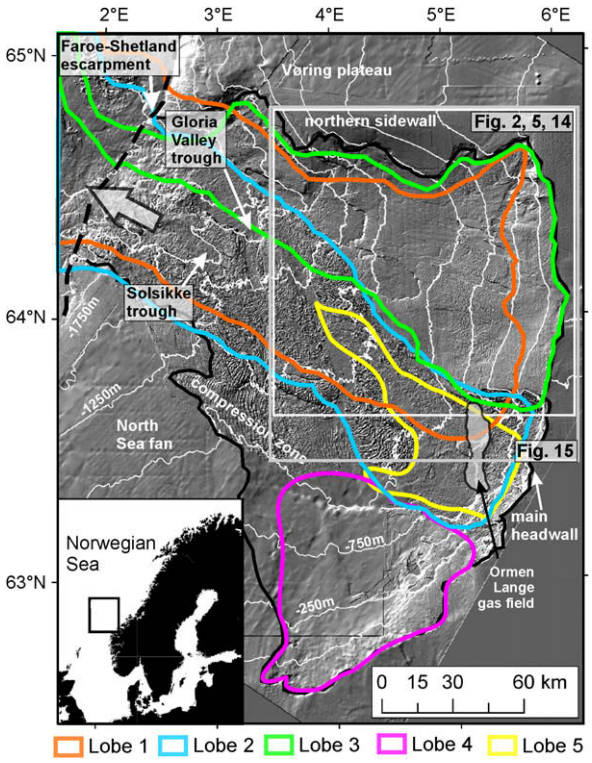


**Fig. 1.** Shaded relief image of the Storegga Slide (illumination from north-east, 5× exaggeration). The solid black line indicates the boundary of the slide scar. Bathymetric contours are at 250 m intervals. The five major slide debris lobes, identified by Haflidason et al. (2004), are superimposed on the shaded relief image. The block arrow denotes the direction of sediment movement. The boundary of Fig. 2 defines the study area.

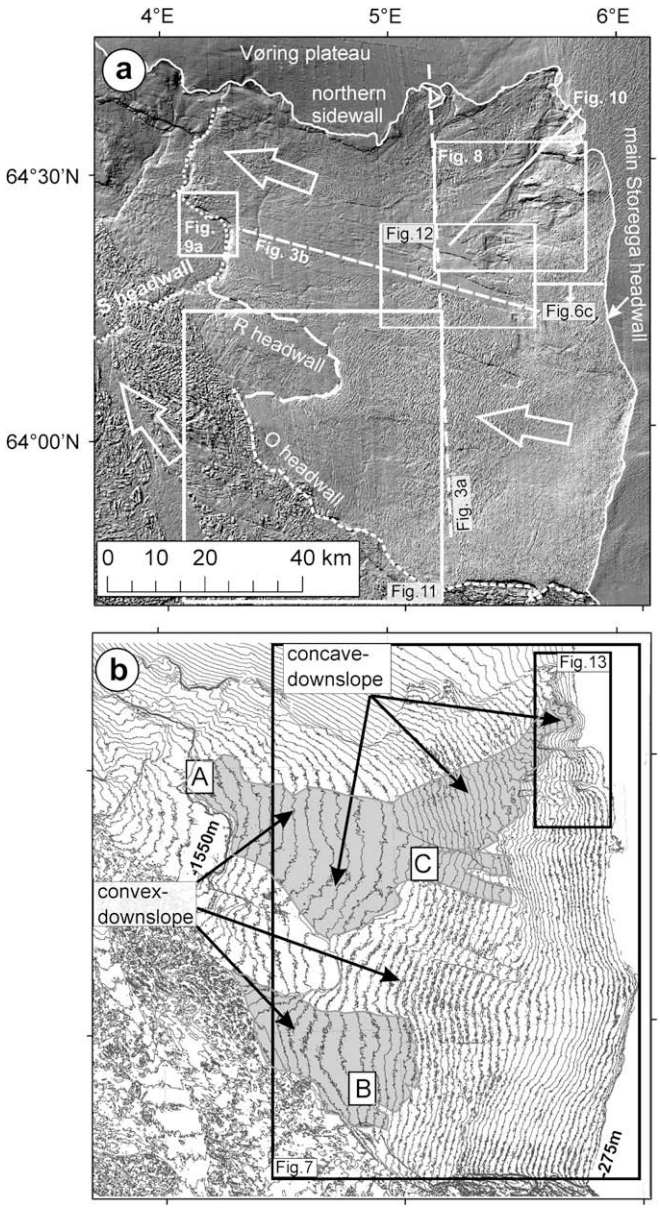


**Fig. 2.** (a) Shaded relief image of the study area in the north-eastern Storegga Slide scar (illumination from north-east, 5× exaggeration). The block arrows denote the direction of sediment movement. The O and R headwalls are glide plane jumps to different stratigraphic levels within the Naust Formation during the retrogressive development of the Storegga Slide. The S headwall is an older feature. The names of these headwalls are taken from the sedimentological unit making up the upslope slip surfaces that are cut by the headwall scarps. (b) Bathymetric contour map of the study area at 25 m intervals. The zone of smooth terrain A and B, and the debris slides (C), are shaded in grey. The distribution of convex- and concave-downslope contour deflections indicates first order erosional and depositional provinces, respectively.

Failure in the study area mainly occurred in the O unit (200–8 ka), the youngest unit of the Naust Formation (Fig. 4). The Naust Formation encompasses a thick, low-angle wedge of clastic sediments and stratified units of Plio-Pleistocene age that overlies the older Kai and Brygge Formations (Bryn et al., 2005a). The Naust sedimentary sequence is characterised by pronounced changes in lithology because its development was controlled by the Fenno-scandian ice sheet growth and retreat patterns (Laberg et al., 2002). The deepest sub-units within the O unit are the O4–O7 sediment sub-units (200–130 ka). These units are glacial tills or debris flow deposits that consist of diamicton with shell fragments and a variable content of gravel and large clasts (Berg et al., 2005). The O3 sediment sub-unit (130–30 ka), emplaced by glacimarine and contouritic deposition, comprises silty clay with sand, scattered gravel and shell fragments. The O1–O2 sediment sub-units (30–15 ka) are made up of unsorted silty, sandy and gravely clay deposited as basal and deformation till. The O3 sediment sub-unit has higher clay and water content, and lower unit weight and sand and gravel content than the other sediment sub-units. For more detailed information about the stratigraphy of the Storegga Slide, the reader is referred to Berg et al. (2005).

## 3. Materials and methods

Three high-resolution acoustic data sets are available for the study area. The bathymetric data set covers the Storegga Slide seafloor from the main slide headwall at the continental shelf edge (~200 m depth) down to a water depth of ~2700 m. These data have a horizontal resolution of 25 m. The bathymetric data is a compilation derived from multibeam echosounder data and seafloor picks of 3D seismic data. The second data set consists of Towed-Ocean-Bottom-Instrument (TOBI) sidescan sonar imagery that covers ~50% of the study area with a nominal horizontal resolution of 6 m. The third data set comprises a series of 2D seismic lines and a 3D seismic cube. The 2D seismic lines, with a horizontal sampling density of 6.25 m and a vertical resolution of ~2 m, are located across the main headwall. The exploration-type 3D seismic data have a 25 m bin spacing and ~5 m vertical resolution near the surface. The 3D seismic data cover an area of 2000 km$^2$ across the northern sidewall.

A suite of geomorphometric techniques for the quantitative characterisation of bathymetric data has been put forward by Micallef et al. (2007b). A number of them were applied to our bathymetric data set. Initially, a shaded relief map and slope gradient map were produced for the study area. The first technique involved the generation of a standard deviation of slope gradient map, which can be used to measure components of surface roughness. This map was produced for grid cells of 1 km$^2$ in area.

The second technique entailed the production of a geomorphometric map, where a landscape is decomposed into its most elementary morphological units. These units, which include breaks and changes of slope, were automatically extracted as lineaments.

The third technique was ridge characterisation. A ridge pattern was automatically extracted from the bathymetry data by implementing a runoff simulation technique. Three morphological characteristics were then determined from the ridge pattern: (a) trough depth, which is the difference in elevation between a trough and the two adjacent ridge crests; (b) ridge length, which is the mean length of individual ridge crests; and (c) ridge spacing, the mean perpendicular distance between ridge crests. The calculations of the mean ridge length and spacing were carried out for grid cells 1 km$^2$ in area.

The fourth technique was ISODATA (Iterative Self-Organising Data Analysis Technique), which is an unsupervised clustering algorithm that defines natural groupings of multivariate data in attribute space. The data layers input into this classification algorithm were trough depth, ridge length, ridge spacing and the standard deviation of slope gradient map. A thematic map with five classes of seabed morphology was generated by ISODATA. As some parts of the map were dominated by scattered cells, a majority filter was applied to produce a continuous coverage.

All these geomorphometric techniques were implemented in ArcGIS Version 9.1. The results of the geomorphometric techniques were integrated with the sidescan sonar and seismic data to characterise the morphology of the seabed and map the submarine mass movements in detail.

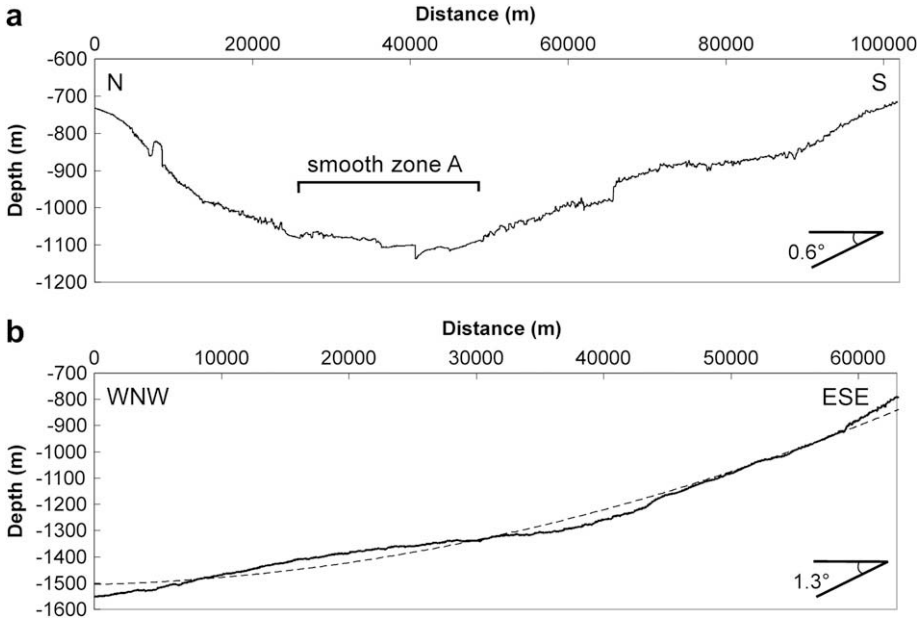


**Fig. 3.** Bathymetric profiles across the study area, oriented (a) north-south and (b) west–north-west to east–south-east. In (b), the dotted line is the polynomial trend line fitted to the elevation data.

## 4. Results

### *4.1. Ridge and trough morphology*

#### *4.1.1. Spreading*

Spreading is a type of mass movement whereby a sediment unit is extended and broken up into coherent blocks that are displaced and tilted along a planar slip surface. The morphological signature of spreading is a repetitive pattern of parallel to sub-parallel ridges and troughs that are oriented perpendicular to the direction of sediment movement. The occurrence and dynamics of spreading within the Storegga Slide have been investigated by Micallef et al. (2007c), who identified loss of support and seismic loading as the most likely triggers of this mass movement.

Ridge and trough morphology is the most common morphology within the study area. Ridges and troughs cover >4000 km$^2$ of the

| Unit | Sub-unit | Age (Ma) | Lithology |
|---|---|---|---|
| Naust O | O1 | 0.024 - 0.008 | Unsorted silty, sandy, gravely clay with shell fragments |
| | O2 | | |
| | O3 | 0.13 - 0.024 | Silty clay with sand, scattered gravel and shell fragments |
| | O4 | 0.2 - 0.13 | Diamicton with shell fragments and variable content of gravel and larger clasts |
| | O5 | | |
| | O6 | | |
| | O7 | | |
| Naust R | R1 | 0.38 - 0.2 | Silty clay with little sand and gravel |
| | R2 | | |
| | R3 | | Increasing sand and gravel compared to R2 |
| Naust S | S1 | 0.7 - 0.38 | Silty clays with variable content of sand, gravel and shell fragments |
| | S2 | | |
| | S3 | | |
| | S4 | 1.1 - 0.7 | |
| | S5 | | |
| | S6 | | |
| Naust U | U1 | >1.1 | Unsampled |
| | U2 | | |

**Fig. 4.** Stratigraphic framework and lithology of the Naust Formation. (source: adapted from Berg et al., 2005).

study area as a continuous pattern that extends from the main headwall down to the S headwall (Fig. 5). The ridges and troughs are mainly concave-downslope or linear in plan. The ridges have a mean length and spacing of 334 m and 287 m, respectively; the mean trough depth is 3.1 m. Spreading across the study area occurs within the O3 sediment sub-unit (Micallef et al., 2007c).

*4.1.2. Spreading model*

Micallef et al. (2007a,c) proposed a model representing the failure dynamics of spreading within the study area. This model entails failure in a thin slab of sediment underlain by a quasi-planar failure plane. The slab is under tension and ruptures into a series of coherent blocks, with shear planes dipping upslope (Fig. 6a). These blocks translate and tilt downslope along the failure plane. This mode of failure is the result of extensional forces that are higher downslope and basal resisting forces that are stronger upslope, and is different from the mode of failure proposed by Kvalstad et al. (2005) for the Ormen Lange region. The dissimilarity in the modes of failure is attributed to the different physical properties of the failing sediment (Micallef et al., 2007c).

Mechanical modelling was carried out to understand the behaviour of the spreading blocks within the study area (Micallef et al., 2007a,c). First, the resultant force acting on a single block was calculated in 2D by deducting the resisting forces from the driving forces prior to detachment and translation:

$$\text{Driving force prior to detachment} = \sin\theta(\gamma Sl) \quad (1)$$

$$\text{Resisting forces prior to detachment} = \tan\phi[\gamma Sl(\cos\theta - u] + c + P \quad (2)$$

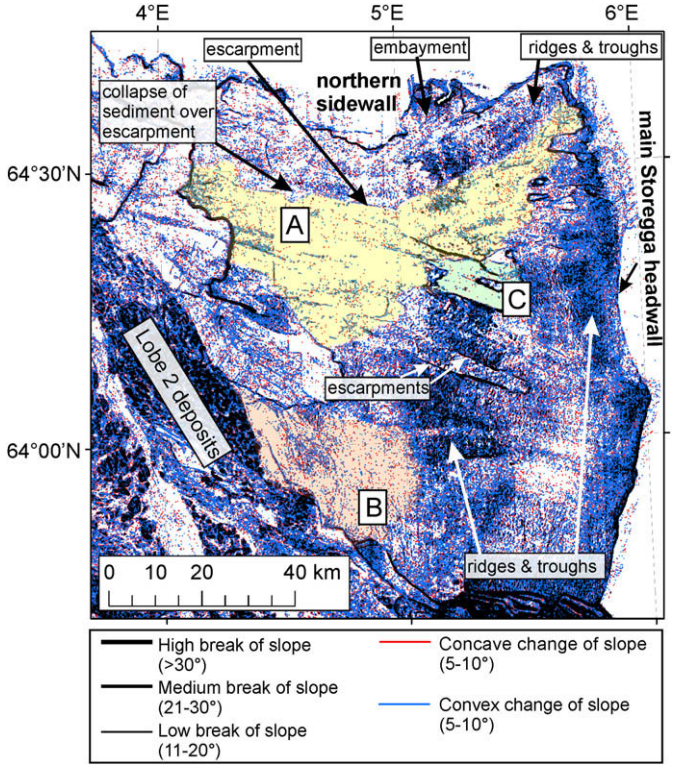


**Fig. 5.** Geomorphometric map of the study area. The zones of smooth terrain A, B and C are shaded in yellow, pink and green, respectively. The escarpment defining the northern boundary of the downslope section of zone A consists of a change of slope (For interpretation of the references to colour in this figure legend, the reader is referred to the web version of this article.).

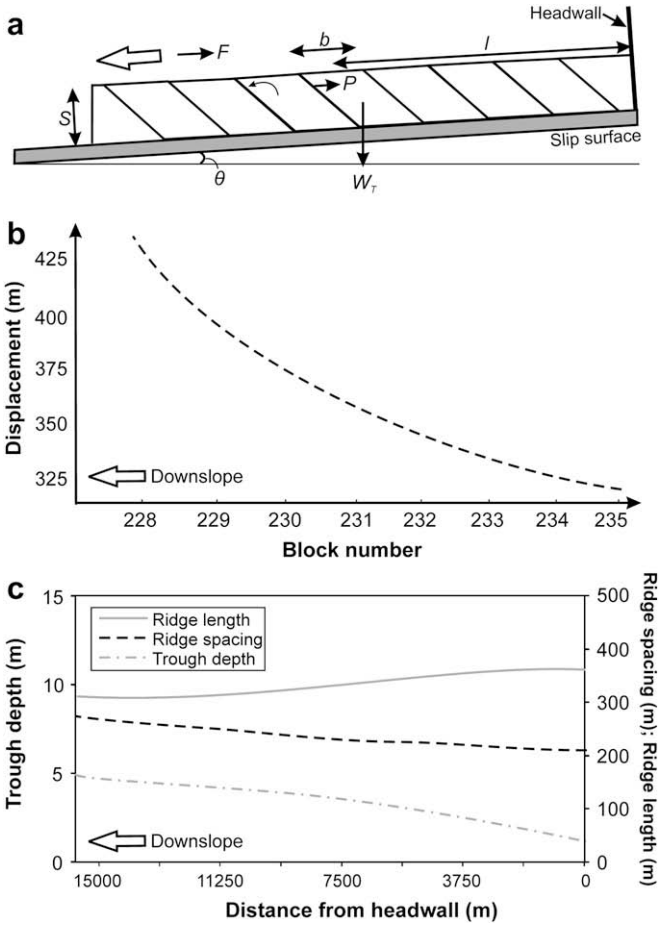


**Fig. 6.** (a) Schematic illustration of the mechanical model of submarine spreading proposed by Micallef et al. (2007c). (b) Plot of absolute block displacement vs. block number generated by the mechanical model for spreading within the study area (source: adapted from Micallef et al., 2007a). The block number indicates the order in which a group of blocks in an upslope section of the slope is displaced. (c) Polynomial trend lines fitted to changes in ridge and trough morphological characteristics with distance from headwall across part of the study area. Location of (c) is shown in Fig. 2a.

where $\gamma$ is the submerged unit weight; $S$, sediment unit thickness prior to failure; $l$, distance from headwall; $\theta$, slope gradient of slip surface; $\phi$, angle of internal friction; $u$, pore water pressure; $c$, resisting force due to cohesion; and $P$, supporting force from slab downslope.

Since loss of support is considered the most likely trigger of spreading within the Storegga Slide, the spread in the mechanical model was triggered by the removal of a block in the distal part of the slope and the corresponding reduction of $P$ to 0.

Equations of motion were then employed to calculate the maximum velocity achieved and the distance covered by the block. The resultant force acting on the block during translation was calculated by deducting the resisting forces from the driving forces using the following equations:

$$\text{Driving forces during translation} = \sin\theta(\gamma Sb) \quad (3)$$

$$\text{Resisting forces during translation} = F \quad (4)$$

where $b$ is the width of block and $F$, the fluid resistance and friction at the base of the block.

The assumptions of this model are that failure is instantaneous and that fluid resistance and friction at the base are constant along the entire slip plane of the spread. The values for the parameters in the model were estimated from a ~35 km long section of seismic

data across the main headwall of the Storegga Slide as well as from published data. $b$ is 130 m (a total of 269 blocks over 35 km were considered) and $S$ is constant at 80 m. The other parameters were considered to change linearly from the headwall to the distal part of the spread in the following way: (i) $\theta$ changes from 1° to 0.96°; (ii) $\gamma$ and $\phi$ change from 10 kN m$^{-2}$ and 27.5° to 9 kN m$^{-2}$ and 25°, respectively; (iii) pore pressure decreases from 1000 kN m$^{-2}$ to 600 kN m$^{-2}$. $c$ is known to be constant (Sultan et al., 2004b) across the study area whereas $F$ is assumed to be constant; both parameters were assigned an arbitrary value.

The values of the model parameters in the distal part of the slope generate the highest possible resultant force and therefore the highest maximum velocity and block displacement after slope failure. For successive blocks upslope, the values of the model parameters change, resulting in a lower resultant force, lower maximum velocity and lower block displacement after slope failure. The change in block displacement with distance downslope is an exponential increase (Fig. 6b). This corresponds to the ridge displacement pattern empirically estimated from the seabed of the Storegga Slide (Fig. 12 in Micallef et al., 2007c).

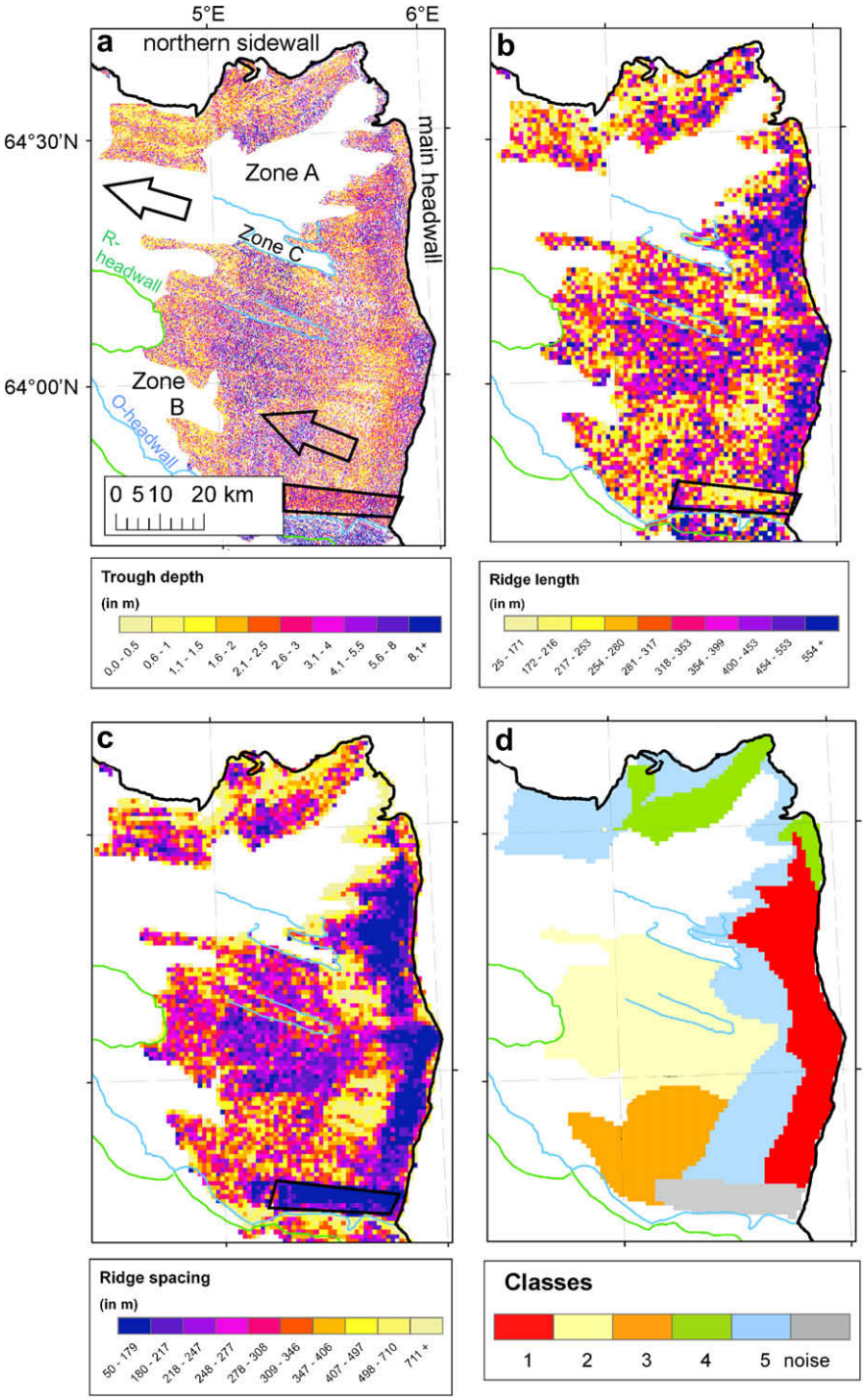


**Fig. 7.** (a) Trough depth; (b) ridge length and (c) ridge spacing maps extracted from the areas where spreading occurs in the study area. Noise due to merging of data of different resolution is enclosed by a black rectangle. (d) ISODATA classification thematic map, which divides spreading within the study area into five classes. Some parts of the thematic map were dominated by scattered cells, so a majority filter was applied to produce a continuous coverage.

**Table 1**
Mean (and standard deviation) of the ridge and trough morphological characteristics for the five different classes identified by the ISODATA classification technique.

| | Trough depth (m) | Ridge length (m) | Ridge spacing (m) |
|---|---|---|---|
| Class 1 | 3.8 (±1.0) | 434 (±147) | 192 (±52) |
| Class 2 | 5.4 (±1.2) | 336 (±115) | 286 (±92) |
| Class 3 | 5.5 (±1.0) | 303 (±112) | 332 (±104) |
| Class 4 | 3.5 (±0.9) | 320 (±136) | 396 (±222) |
| Class 5 | 1.2 (±0.9) | 292 (±114) | 517 (±320) |

Changes in ridge morphology with distance downslope for a 15 km section of the seabed (Fig. 6c) complement the displacement pattern observed in Fig. 6b. Ridge spacing and trough depth increase with distance from the headwall, whereas ridges become progressively shorter in this direction. These changes in ridge morphology indicate that the spreading blocks undergo increasing displacement, fragmentation, deformation and tilting with distance downslope. This is accompanied by progressive thinning of the spreading sediment and lowering of the seabed (Micallef et al., 2007c). A gentle headwall is formed at the upslope limit of the spread where the driving and resisting forces reach equilibrium.

*4.1.3. Spatial variations in ridge and trough morphology*

The ridge and trough morphology across the entire study area was divided into five main classes using the ISODATA classification technique described in Section 3 (Fig. 7d). The ridge and trough morphological characteristics for each class are listed in Table 1. According to the spreading model proposed by Micallef et al. (2007c), the thematic map in Fig. 7d should show a progressive change from class 1 to class 2 and then to class 3 with increasing distance from the main headwall. In this direction, ridges should become shorter, ridge spacing should increase and troughs should become deeper. This is not the case, however (Fig. 7d). In the southern half of the spreading zone, this pattern is disrupted by class 5. Class 5 is located between classes 1 and 2 and consists of the shallowest troughs, shortest ridges and largest spacing. The ridge and trough morphology along the northern sidewall is also different to that predicted by the spreading model. Classes 4 and 5 dominate this region, where ridges are shorter and more spaced when compared to the ridges at the same distance from the main headwall in the southern half of the spreading area. The south-western part of the study area, covered by class 3, has shorter ridges, higher ridge spacing and deeper troughs than the adjacent terrain to the north (class 2).

*4.2. Discontinuity in ridge and trough morphology*

The ridge and trough morphology is not spatially continuous across the entire study area (Fig. 5), but it is disrupted by: (i) a zone of smooth seabed in the north-eastern to central northern part of the study area (zone A); (ii) a zone of smooth seabed in the south-west of the study area (zone B); (iii) two elongated areas of smooth seabed in the central part of the study area (zone C); and (iv) a number of windows. A window is a part of the slide scar where the underlying slip surface has been exposed.

*4.2.1. Zone of smooth seabed in the north-eastern to central northern part of the study area (zone A)*

*4.2.1.1. Morphology.* Zone A is an extensive region of smooth terrain in the north-eastern to the central northern part of the study area that contrasts with the adjacent ridges and troughs, and the blocky morphology elsewhere in the slide scar (Figs. 2b, 5, 8). Zone A has a total area of 2380 km$^2$ and covers a depth range from 530 to 1550 m, over which the mean slope gradient is 1.08°. The border of the smooth zone is characterised by either a very gentle or

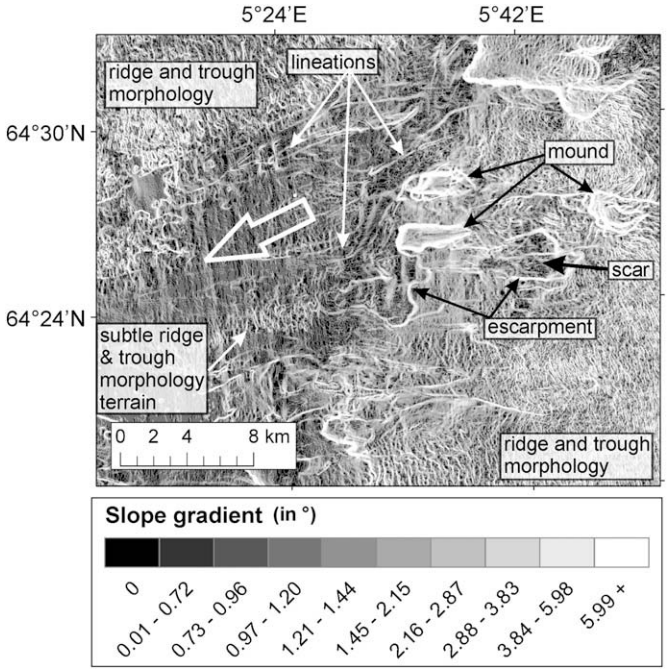


**Fig. 8.** Slope gradient map of the north-eastern zone A. The location of lineations, escarpments, elongated subtle ridge and trough morphology is indicated. The block arrow denotes the direction of sediment movement.

no change in slope. In the downslope half, however, zone A is slightly deeper than the surrounding spreading area, and at the northern border of zone A there is a 35 km long escarpment (Fig. 5). This escarpment is up to 15 m high. In some areas, the spread sediments from the north collapse over this escarpment into zone A (Fig. 5). The northern border of zone A is mostly oriented parallel to the northern sidewall, as is the general movement direction of the spreading ridges and troughs in this part of the Storegga Slide. In general, the bathymetric contours in zone A are convex-upslope, suggesting sediment evacuation (Fig. 2b). This contour pattern changes in the downslope half of zone A, where the contours are convex-downslope in the northern part, implying sediment deposition (Fig. 2b). A bathymetric profile trending downslope across zone A has a gross form that is concave upwards with a generally steeper upslope section, and a more gently sloping lower section (Fig. 3b). The distal part of the profile, which is convex upwards in shape, shows relatively elevated terrain (Fig. 3b). This corresponds to the convex-downslope contours in this area and denotes deposition (Fig. 2b).

There are a number of prominent morphological features within zone A:

(i) *Escarpments*: a number of shallow escarpments are located in the upslope and midslope sections of zone A. Most of these escarpments are linear and trend perpendicular to the contours, although some of them are arcuate, contour-parallel and concave-downslope in plan (Fig. 8). A few linear and saw-tooth escarpments can also be identified. The escarpments are up to 30 km long and have a maximum height of 35 m. Some form headwalls for deep and smooth scars. Two long escarpments extend south-east into the southern half of the spreading area (Fig. 5). Between these escarpments, spreading has occurred along a deeper slip surface than in adjacent areas.
(ii) *Elongated areas of subtle ridge and trough morphology*: small areas of ridges and troughs, with troughs that are shallower than those in the surrounding spreads, can be observed within zone A (Fig. 8). These areas have positive relief and are

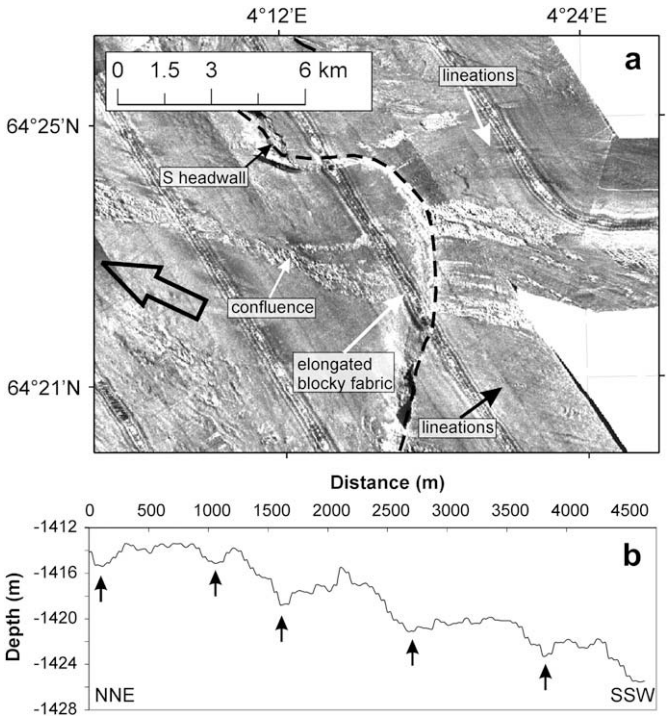


**Fig. 9.** (a) TOBI sidescan sonar image from the downslope section of the study area showing lineations and elongated blocky terrain across the S headwall. (b) A bathymetric profile across lineations in Fig. 12b. The small black arrows indicate the narrow and shallow furrows.

elongated in a downslope direction. They are up to 7 km wide and 15 km long.

(iii) *Elongated blocky terrain*: zone A is also characterised by a number of long, narrow, downslope-oriented areas of positive relief blocky fabric (Fig. 9a). These areas are up to 7.5 km wide and 45 km long. They are concentrated in the downslope section of zone A and extend across the S headwall, where the elongated areas of the blocky terrain converge (Fig. 9a). These features begin directly downslope from the escarpments.

(iv) *Lineations*: numerous lineations oriented perpendicular to the bathymetric contours are observed across most of zone A (Figs. 8, 9a). The lineations are generally parallel to each other, although some convergence occurs upslope. The lineations are up to 45 km long and 300 m wide, and they have the same trend as the elongated areas of subtle ridges and troughs and the blocky terrain. The lineations have a modest topographic expression as narrow furrows with a maximum depth of 3 m (Fig. 9b). Most lineations can be traced back upslope to an escarpment or the main headwall. Some lineations can also be observed in the spread areas. A number of lineations terminate within spreading class 5.

*4.2.1.2. Internal architecture.* The seismic character of the Plio-Pleistocene Naust Formation in zone A is illustrated in Fig. 10. The seabed is characterised by a gently sloping, high amplitude reflector that is interrupted by a step at the main headwall. Upslope of the headwall, the seabed is shallower and partly consists of a number of upslope and downslope dipping segments, which correspond to a spread of limited extent associated with the headwall. Here, the seismic facies beneath the seabed reflector is thick, generally transparent and is underlain by a strong high amplitude reflector that extends across the entire seismic profile. The seismic facies between the seabed reflector and the strong high amplitude reflectors upslope of the headwall scarp is interpreted as representative of the O1–O7 sediment sub-units. The strong, high amplitude reflector is interpreted as the INO7 horizon, which is the base of the O7 sediment sub-unit (Berg et al., 2005). The O1–O7 sediment sub-units are dissected by a thin, high amplitude reflector, which is interpreted as the INO3 horizon at the top of the O4 sediment sub-unit. The O3 sediment sub-unit, which is known to pinch out at the main headwall, is not visible (Berg et al., 2005). The sediments above the INO3 horizon are therefore interpreted as the O1–O2 sediment sub-units, whereas those underneath are the O4–O7 sediment sub-units.

The sediments within the slide scar show a chaotic seismic facies with some weak internal reflectors (Fig. 10). This facies extends from the main headwall down to the south-west end of the seismic profile. The facies becomes thinner in this direction and we interpret it as a debris flow consisting of O unit sediments. In the south-western half of the seismic profile, the chaotic facies is underlain by a series of parallel, high amplitude reflectors (Fig. 10). These are interpreted as contourite drift deposits of the R1–R2 sediment sub-units, which are thought to have formed the failure

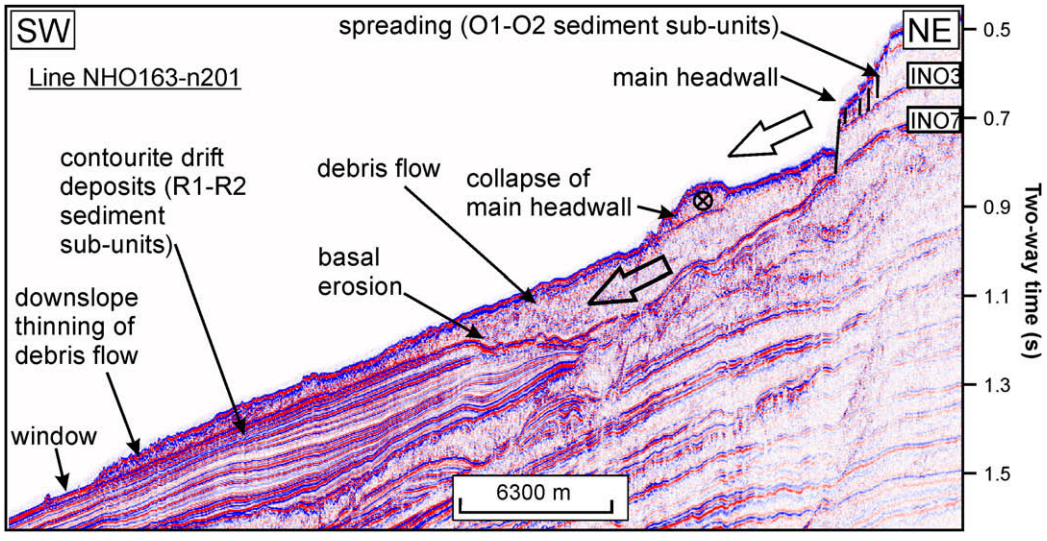


**Fig. 10.** Seismic dip profile across the slide scar in zone A and the main headwall. Location of profile is shown in Fig. 2.

surface on which the debris flow failed. The failure surface is exposed as a window in the south-western part of the seismic profile (Fig. 10).

An alternative interpretation of the seismic profile shown in Fig. 10 is that the debris flow consists entirely of O4–O7 sediment sub-units and is older than the Storegga Slide. This interpretation is supported by the fact that the seismic character of the O4–O7 sediment sub-units is chaotic both upslope of the headwall and within the slide scar. On the other hand, no sharp sediment thickness variations or onlaps could be observed in the near surface sediments in the 3D seismic data. In fact, these surface sediments drape Storegga-related mass movements further south. Also, there is no clear boundary between debris flows of potentially different ages in Fig. 10.

#### 4.2.2. Zone of smooth seabed in the south-western part of the study area (zone B)

A second zone of smooth terrain is located in the south-west of the study area, bordering the ridge and trough morphology (Figs. 2b, 5, 11a). This zone has an area of 450 km$^2$, is characterised by convex-downslope contours (Fig. 2b), and its seafloor is 10–20 m deeper than the adjacent area of ridges and troughs. The smooth terrain is disrupted by long, deep troughs oriented north-south, as well as downslope-oriented lineations and contour-parallel escarpments (Fig. 11a). A small area of distinct positive relief is located to the south of zone B, between the O and R headwalls (Fig. 11a). The surface of this area is characterised by a well-defined pattern of long, convex-downslope ridges and troughs. The seismic dip profile in Fig. 11b demonstrates that the seismic character of the seabed in zone B is characterised by a continuous high amplitude reflector. A chaotic seismic facies 60–70 ms (TWT) thick occurs beneath this reflector. This contrasts with the segments of upslope and downslope dipping reflectors in the spreading area to the east. A number of blocks of parallel, high amplitude reflectors can be identified within the chaotic seismic facies (Fig. 11b).

#### 4.2.3. Two elongated areas of smooth seabed in the central part of the study area (zones C1 and C2)

Two parallel and elongated areas of smooth seabed (labelled C1 and C2 in Fig. 12a) are located at the southern border of zone A (Fig. 5). These are bordered by parallel, steep, north-west to south-east oriented escarpments, which have a maximum height of 35 m, and a shallow north-south oriented escarpment at the upslope boundary of zones C1 and C2. The areas are up to 3.8 km wide and extend into the ridge and trough terrain upslope. Lineations can be observed both within and downslope of zones C1 and C2 (Fig. 12b). 3D seismic data reveal that zone C1 is characterised by a smooth high amplitude surface reflector (Fig. 12c). This is underlain by a 67 ms (two-way time (TWT)) deep high amplitude seismic reflector, which is parallel to the underlying seismic reflectors (Fig. 12c and c). The seismic facies between the two high amplitude seismic reflectors consists of a series of parallel, low amplitude seismic reflectors and its thickness decreases in a downslope direction. A convex snout is located at the downslope limit of zone C1, underneath which the seismic facies is the thickest and consists of upslope and downslope dipping reflectors. The seismic character of zone C2 is very similar to that of zone C1, although a convex and thick snout is not visible.

#### 4.2.4. Windows

A number of windows are located downslope of pronounced ridges and troughs in the western downslope limit of the spreading areas (Fig. 12b).

### 4.3. Elongated embayment

North of zone B, the R headwall is characterised by an elongated embayment trending north-west to south-east (Fig. 11a). The embayment is 33 km long and 15 km across. The walls of the embayment are steep and ~60 m high. The seabed between these walls is characterised by downslope-trending lineations and

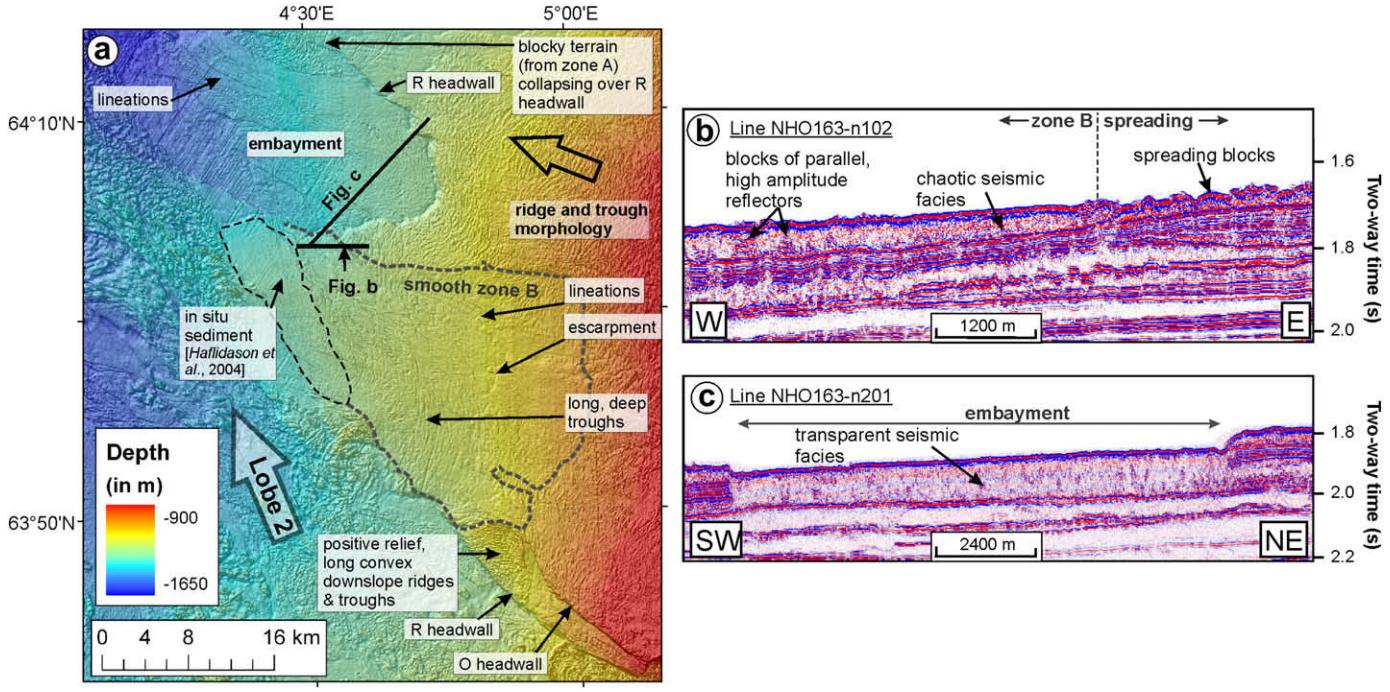


**Fig. 11.** (a) Bathymetry draped on a shaded relief map of zone B and the elongated embayment (illumination from north-east, 5× exaggeration). Zone B is enclosed by a grey dotted line. The main morphological features are labelled. (b) Labelled seismic dip profile across the northern part of zone B and the adjacent spreading terrain. (c) Labelled seismic dip profile across the elongated embayment.

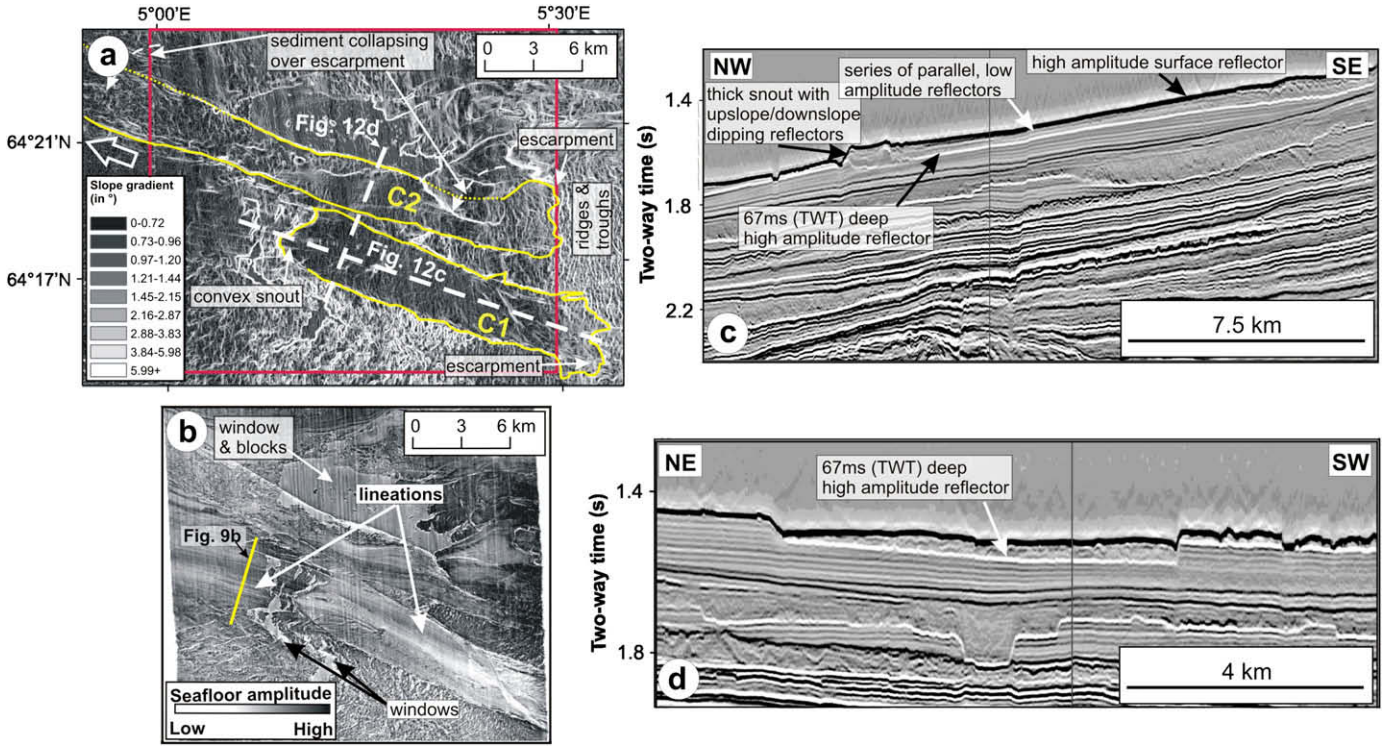


**Fig. 12.** (a) Slope gradient map of zones C1 and C2 (outlined in a solid yellow line) in the central part of the study area. (b) Seismic amplitude map of the seabed enclosed by a solid red square in (a). The lineations and windows are clearly visible. (c, d) Seismic dip profiles across zone C1. The location of these profiles is shown in (a).

a subtle blocky morphology. The ridges and troughs located upslope of the embayment are convex-upslope in plan and parallel to the embayment wall (Fig. 11a). Some of the blocky terrain identified within zone A extends into the embayment across the northern wall (Fig. 11a). The downslope part of the southern wall is covered by large blocks of debris. The seismic dip profile within the embayment shows a continuous, smooth, high amplitude reflector (Fig. 11c). This is underlain by a 136 ms (TWT) thick transparent and homogeneous seismic facies. The flanks of the embayment are underlain by a series of parallel, high amplitude reflectors. The morphology and the seismic character of the embayment are very similar to those of the Solsikke and Gloria Valley troughs in the distal part of the Storegga Slide scar (Riis et al., 2005) (Fig. 1).

### 4.4. Headwall morphology

In the study area, the main Storegga headwall can be divided into two sections. The northern section, which is 26.5 km in length, is characterised by an abrupt concave break of slope, upslope of which is located a gentler convex break of slope, with spreading ridges and troughs found in between (Fig. 13). The headwall has a mean height of 72 m and features a number of narrow embayments. This section of the main headwall is located upslope of zone A and spreading class 4 south of the northern sidewall (Fig. 7d). In the southern section, the main headwall is located upslope of spreading ridges and troughs in class 1 (Figs. 7d, 13). It consists of a very gentle convex break of slope, where ridges and troughs grade into a gentle undisturbed slope in an upslope direction. The mean headwall height for the southern section is 24 m, although heights of 50 m are recorded in the southern half of this section.

The northern sidewall generally consists of an abrupt break of slope that is up to 50 m high (Figs. 2, 5). The upslope half of the northern sidewall is disrupted by a deep embayment that is ~15 km wide and extends 9 km upslope into the northern sidewall (Fig. 5). The terrain in this embayment consists of ridges and troughs that we attribute to spreading in a south-west direction. The morphology of these ridges and troughs is similar to those in spreading classes 4 and 5 (Figs. 5, 7d). The ridge and trough morphology in the embayment is broken up by a number of downslope-oriented lineations. The areas upslope of the northern sidewall in this embayment are also affected by spreading, although they are characterised by a more closely spaced pattern of shallow ridges and troughs.

### 4.5. Pockmarks

Pockmarks are seafloor depressions resulting from the expulsion of fluids (Judd and Hovland, 1992; Bouriak et al., 2000). They are very common on the undisturbed seafloor north of the Storegga slide scar area (Bünz et al., 2003) where they are concentrated in a narrow band striking west–north-west to east–south-east. This extends from the northern sidewall to an area upslope of the northern section of the main headwall (Bouriak et al., 2000; Bünz et al., 2003) (Fig. 14).

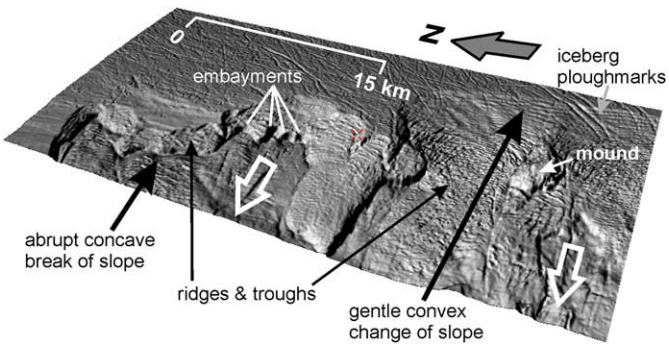


**Fig. 13.** 3D shaded relief bathymetry (illumination from north-east, 5× exaggeration) showing the two different morphologies of the main headwall upslope of zone A.

## 5. Discussion

### 5.1. Interpretation

#### 5.1.1. Spatial variation in ridge and trough morphology

Spreading classes 3 and 5 in the southern half of the study area, and classes 4 and 5 south of the northern sidewall, do not fit into the morphology expected for a typical submarine spread (Fig. 7d). These classes have shorter ridges, higher ridge spacing and shallower troughs than would be expected based on observations elsewhere in the slide area. By interpreting these morphological characteristics in the context of the spreading model of Micallef et al. (2007c), we hypothesise that classes 3, 4 and 5 are indicative of higher displacement and remoulding of the spreading blocks along the northern sidewall and in the southern half of the spreading areas, in comparison to the spreading areas elsewhere (Fig. 14).

#### 5.1.2. Zones of smooth terrain

*5.1.2.1. Zone A.* The smooth terrain and the numerous escarpments, lineations and elongated zones of blocky terrain and ridges and troughs within zone A contrast with the surrounding areas of ridge and trough morphology. We interpret the morphology within zone A as having been formed by debris flows that were later overprinted by turbidity currents. In our interpretation, the escarpments are the sidewalls and headwalls of debris flows (Fig. 14). The lineations correspond to narrow furrows and many can be traced back to the headwalls. The furrows may have two different origins: they have either been eroded into the underlying failure surface by turbidity currents, or they were formed at the base of individual debris flows (Figs. 9, 14). In spreading classes 4 and 5, the furrows may have been formed by turbidity currents evolving from spreads in areas of high displacement and remoulding, although they could also be later features, with the terrain adjacent to the main headwall acting as the source area of the turbidity currents.

The elongated blocky terrain in zone A is interpreted as residual debris flow deposits (Fig. 9). The deposits are located downslope of the headwalls and they are concentrated in the distal part of zone A. The grading from a furrowed seafloor to a field of longitudinal deposits indicates that the flow regime decreases gradually downslope. Changes in the contour shape within zone A from convex-upslope to convex-downslope confirm this change from an erosional to depositional flow regime (Fig. 2b). The zones of subtle ridges and troughs within zone A are interpreted as remnant morphology originally formed by spreading that has survived in areas that have subsequently been remobilised by debris flows (Figs. 8, 14). The presence of these remnants suggests that spreading initially extended over part or all of zone A. It has already been established that lobe 1 eroded the O1–O2 sediment sub-units and that spreading occurred in the O3 sediment sub-unit (Haflidason et al., 2004; Micallef et al., 2007c). The absence of the latter from within the slide scar and the presence of the remnant spreading morphology may indicate that the debris flows and turbidity currents remobilised or removed the spreading blocks formed in the O3 sediment sub-unit. Erosion by turbidity currents sourced higher on the slope and/or remobilisation of material within zone A by debris flows would explain the generally smoother, deeper terrain and the thinner Storegga slide sediments in zone A, in comparison to the surrounding spreading areas (Figs. 2a, 8, 14). Some of these turbidity currents and debris flows may have been sourced by local failures along the main headwall; they could thus be responsible for the irregular morphology of the main headwall upslope of zone A (Fig. 13). The fact that the seismic facies of the sediment inside the slide scar in Fig. 10 is generally more chaotic than the O4–O7 sediment sub-units upslope of the headwall indicates that debris flows have also mobilised the O4–O7 sediment sub-units themselves. The deformation of the O4–O7 sediment sub-units is also confirmed by the localised plastic deformation of the sediment in the midslope section of zone A, as indicated by the collapse of smooth sediment lobes across the northern sidewall of zone C (Figs. 12, 14).

*5.1.2.2. Zone B.* The morphology of zone B is similar to that of zone A. The smooth terrain, lineations and escarpments within zone B may all be indicative of sediment mobilisation in the form of debris flows and turbidity currents. Sediment mobilisation by debris flows is corroborated by the chaotic seismic character of the surface sediment in this area (Fig. 11b). The long and deep troughs oriented north-south within zone B, and the small area of positive relief located outside of zone B, are indicative of compression and transpressive shearing due to the mobilisation of sediment in a north–north-west direction in lobe 2 (Figs. 11a, 14).

*5.1.2.3. Zones C1 and C2.* The seismic reflectors labelled in Fig. 12c and d are interpreted as layers in a contourite drift sediment package, namely the R1–R2 sediment sub-units (Figs. 4, 10). Taking into consideration the morphology and the internal architecture of zone C1, we interpret this zone as a shallow-seated debris slide. The parallel escarpments that define the area of zone C1 are the sidewalls of the slide. The 67 ms (TWT) deep high amplitude reflector is interpreted as a discrete, planar failure surface that follows sediment stratification. This failure surface is deeper than the slip surface for the adjacent spreading sediment (Fig. 12d). The sediment has been mobilised downslope above the failure surface in zone C1. The mobilised sediment is characterised by a low thickness to downslope length ratio and its internal structure is generally undisturbed. Internal deformation of the displaced sediment can only be observed at toe of the slide, as shown by the upslope and

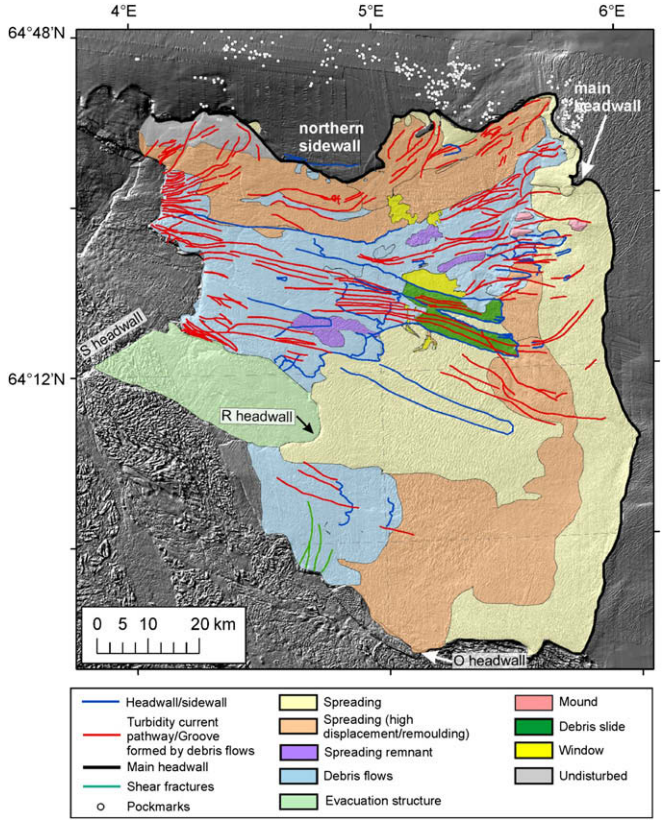


**Fig. 14.** Interpretative map of the mass movements and geological processes that have shaped the north-eastern Storegga Slide scar.

downslope dipping reflectors, which are interpreted as compressional folds and thrusts. The toe is also the thickest part of the slide mass and is considered the accumulation zone of the debris slide. Turbidity currents have left their mark on the surface of the slide in the form of a series of lineations. Zone C2 has a similar morphology and internal architecture to that of zone C1 (Fig. 12a), and we also interpret this feature as a debris slide. The accumulation zone is, however, not clearly identifiable in the bathymetric and seismic data. The northern sidewall of zone C2 is covered by sediments with a subtle, uneven morphology to the west, whereas to the east sediment has collapsed over the escarpment in a lobate form (Fig. 12a).

### 5.1.3. Elongated embayment

The elongated embayment in Fig. 11a is interpreted as an evacuation structure, similar to those identified in the distal part of the Storegga Slide by Riis et al. (2005) (Fig. 14). These authors define evacuation structures as crater-like features that are formed and enlarged by the removal of ooze material during a mass flow. The ooze material is mobilised because of its low density, which enables it to rise to the top and form mounds. The evacuation structure is simultaneously infilled by material from the mass flow. In the case of the evacuation structure in Fig. 11a, the embayment was filled with sediment from the O1–O2 sediment sub-units mobilised by lobe 1, and the O3 sediment sub-unit spreading upslope of the embayment. We propose that the evacuation structure predates spreading because the ridges and troughs upslope of the evacuation structure are convex-upslope in plan and parallel to the escarpment. This indicates that the ridges and troughs were formed due to loss of support at the escarpment. The collapse of blocky sediment from zone A into the evacuation structure implies that the latter also predates the formation of debris flows in zones A and B (Fig. 11a).

## 5.2. Development model for the north-eastern Storegga Slide

Based on the identification of spreading, debris slides, debris flows, turbidity currents, compressional features and an evacuation structure in the study area, we propose a revision of the development model for the north-eastern Storegga Slide suggested by Haflidason et al. (2004) (Figs. 1, 15; Table 2).

In our development model, we accept that the Storegga Slide was most likely triggered in the area close to the S headwall as proposed by Bryn et al. (2005a) and Atakan and Ojeda (2005). Failure developed at the foot of the slope in this region and propagated upslope in an eastern direction. The surface sediment sub-units O1–O2 were removed during the development of event 1a (lobe 1), with the top of the O3 sediment sub-unit acting as the failure surface (Fig. 15). The sediments were deposited as turbidites and debrites in the Norwegian Sea Basin (Haflidason et al., 2004). No deposits from event 1a could be identified in the study area. The surface sediments comprising the O1–O2 sediment sub-units failed as debris flows and turbidity currents because the sediments were deposited during the last glacial–interglacial cycle and had not undergone significant consolidation. Event 1a extended across most of the study area and the region downslope from the S headwall down to the Norwegian Sea Basin (Fig. 15b). The maximum upslope extent of lobe 1 was initially estimated at ~20 km from the main headwall (Haflidason et al., 2004) (Fig. 15a). There are, however, no clear morphological features that define this limit. We therefore infer that event 1a extended up to the main headwall, giving a total area of 40,804 km$^2$ (Fig. 15b). This would explain the 50 m headwall height observed in the southern part of the study area. Consolidation by glacial compaction of O1–O2 sediment sub-units located at the main headwall is inferred to have controlled the upslope limit of event 1a. Loading of the deeper

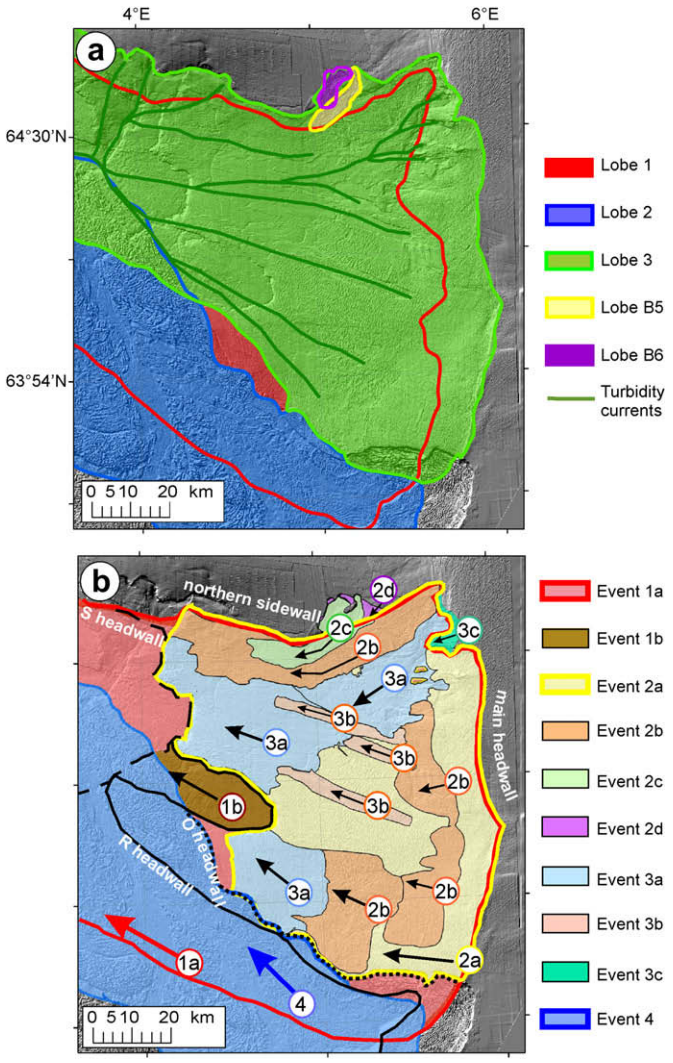


**Fig. 15.** (a) The development model for the north-eastern Storegga Slide proposed by Haflidason et al. (2004), described in terms of lobes. (b) The revised development model proposed in this paper, described in terms of events. The event number implies the stratigraphical relationship, whereas the alphabetical subscripting denotes that the event is part of a group of events within the same stratigraphical order.

sediment in the lower part of the study area by sediment mobilised during event 1a is thought to have led to the formation and infilling of the evacuation structure (event 1b) (Fig. 15b).

Following the development of events 1a and 1b, we propose that spreading (event 2a) took place across the part of the study area previously affected by event 1a. The failure surface was located within the O3 sediment sub-unit, and the spreading blocks were formed in the upper layers of the O3 sediment sub-unit, resulting in a ridge-and-trough morphology (Micallef et al., 2007c). Spreading extended from the S headwall and the evacuation structure up to the main headwall, affecting an area of 6870 km$^2$ and defining the shape of the greater part of the main headwall in the study area as a shallow and gentle escarpment (Figs. 13, 15b). The development of this extensive mass movement was brought to a halt by the more consolidated sediment at the main headwall (Kvalstad et al., 2005; Micallef et al., 2007c). Spreading could have been triggered by either loss of support due to the reactivation of the S headwall, by the formation of the evacuation structure and/or by seismic loading associated with the earthquake that initiated the Storegga Slide (Bryn et al., 2005a; Micallef et al., 2007c). The failure of the O3 sediment sub-unit as a spread rather than as a debris flow or

**Table 2**
Characteristics and stratigraphical relationship of the different events in the revised development model of the Storegga Slide, and corresponding lobes in the model of Haflidason et al. (2004).

| Event | Type of mass movement | Sediment sub-unit/s involved | Area ($km^2$) | Stratigraphical relationship | Lobes in model of Haflidason et al. (2004) |
|---|---|---|---|---|---|
| 1a | Debris flows and turbidity currents | O1–O2 | 40,804 | 1 | 1 |
| 1b | Formation and infilling of evacuation structure | Failed sediment: ooze material; infilling by O1–O3 | 480 | | – |
| 2a | Spreads | O3 | 4770 | 2 | – |
| 2b | Spreads (higher displacement) | O3 | 2100 | | |
| 2c | Spreads, debris flows and turbidity currents | O1–O3 | 247 | | B5/B6 |
| 2d | Spreads | O1–O2 | 27 | | – |
| 3a | Debris flows and turbidity currents | O3–O7 | 2200 | 3 | 3 |
| 3b | Debris slides and spreads | O3–O7 | 290 | | |
| 3c | Spreads | O1–O3 | 62 | | |
| 4 | Debris flow | O1–O7 | 20,278 | 4 | 2 |

turbidity current is attributed to its high consolidation and clay content (Berg et al., 2005; Micallef et al., 2007c). Some spreading blocks have undergone a higher extent of displacement and remoulding (event 2b) compared to the ridges and troughs in event 2a (Figs. 14, 15b), as indicated by the shorter ridges and higher ridge spacing. Event 2b encompasses the area south of the northern sidewall and a north-south trending area ~7 km downslope from the main headwall, totalling an area of ~2100 $km^2$. Minor slope failures in the form of spreads, debris flows and turbidity currents (events 2c and 2d) have occurred in O1–O2 sediments along the northern sidewall, presumably due to loss of support from sediment evacuated within the slide scar by events 1, 2a and 2b. Some of these failures are more recent events than the Storegga Slide, having been dated as 2200–5700 cal yr BP in age (Haflidason et al., 2005).

Event 3 covered the northern central and south-western part of the study area, extending from the S headwall to the main headwall and affecting a total area of ~2500 $km^2$ (Fig. 15b). Event 3a consisted of debris flows and turbidity currents that affected the seabed in zones A and C (Fig. 5). These mass movements deformed or removed most of the ridge and trough terrain formed by event 2 in the O3 sediment sub-unit, and mobilised the underlying O4–O7 sediment sub-units. The presence of spreading remnants within zone A is the key observation that proves that the mass movements in event 3a either post-dated or were coeval with spreading in event 2 (Fig. 14). Debris flows and turbidity currents developed upslope from the S headwall as the headwalls of event 3a mass movements retrogressed in a south-east direction. These mass movements extended into the north-east of the study area where the direction of sediment movement changed from north-west to south-west (Fig. 15b). Loss of support resulting from these flows triggered two debris slides and a spreading event in the central part of the study area (labelled collectively event 3b in Fig. 15b). Loss of support due to removal of sediment by event 3a in the north-eastern part of the slide scar triggered spreading upslope of the main headwall (event 3c) (Fig. 15b).

Event 4 corresponds to lobe 2 in Haflidason et al. (2004) and consists of a large blocky debris flow that is thought to have been initiated with event 1a (Fig. 15). However, sediment in event 4 seems to have been mobilised more slowly because it failed along a deeper slip surface (Bryn et al., 2005a). Event 4 formed a large debris flow that extended into the Ormen Lange region, and retrogressed upslope as a series of spreads characterised by long ridges and deep troughs (Micallef et al., 2007c). The identification of short and shallow ridges and troughs on the top of the larger spreading ridges in the Ormen Lange region is proof that failure in event 4 post-dates events 1 and 2 (Kvalstad et al., 2005; Micallef et al., 2007c). During event 4, we suggest that sediment at the northern flank of the debris flow was compressed against the south-western boundary of the spreading area in event 2a. This is inferred from the presence of transpressive shearing and compression features in the form of long and deep troughs within zone B and the small area of positive relief located just outside of zone B (Fig. 11a).

Although the slide development is explained in terms of temporally and spatially distinct events (Table 2), the Storegga Slide should be regarded as a quasi-simultaneous event (Bryn et al., 2005a).

### 5.3. Geological causes of spatial variation in spreading morphology and the occurrence of debris flows and turbidity currents (events 2b, 2c and 3a)

The study of the spreading ridge and trough morphology indicates that some areas (events 2b and 2c) have undergone higher displacement and remoulding, and some sediments have been removed or deformed by debris flows and turbidity currents (event 3a) (Fig. 15b). Mechanical modelling shows that higher displacement of spreading blocks is achieved by high pore water overpressures, a steep slip surface, high unit weight and thickness, and low angle of friction and cohesion of the failing sediment (Micallef et al., 2007c). Debris flows and turbidity currents, on the other hand, are the result of high pore water pressures, low cohesion and fine sediments, amongst other factors (Mulder and Cochonat, 1996). We can thus put forward two potential geological causes for the distribution of debris flows, turbidity currents, and the higher displacement and remoulding of the spreading blocks in events 2b, 2c and 3a.

#### 5.3.1. Slope instability related to gas hydrates

Gas hydrates are an ice-like compound composed of a gas molecule, generally methane, surrounded by a rigid cage of water molecules (Sloan, 1998). They form at high pressure and low temperature from methane-rich pore water. A BSR (bottom simulating reflector) observed on seismic profiles marks the base of the hydrate zone and is thus used as an indicator for the presence of gas hydrates. The extent of the BSR within the Storegga Slide has been mapped by Bünz et al. (2003). The BSR has a spatial extent of 4000 $km^2$ and it occurs beneath the seabed in water depths of 550–1300 m. Gas hydrates occur continuously along the northern sidewall outside the Storegga Slide and into the north-eastern slide scar area (Fig. 16a).

The role of gas hydrate dissolution and dissociation in activating submarine slope instability has been widely discussed (Paull et al., 2000; Sultan, 2007). At sufficient concentrations, gas hydrates may cement the sediments, increasing their strength, or fill the voids and prevent normal sediment compaction, destabilising the sediments once the hydrates dissolve/dissociate (Sultan et al., 2004b).

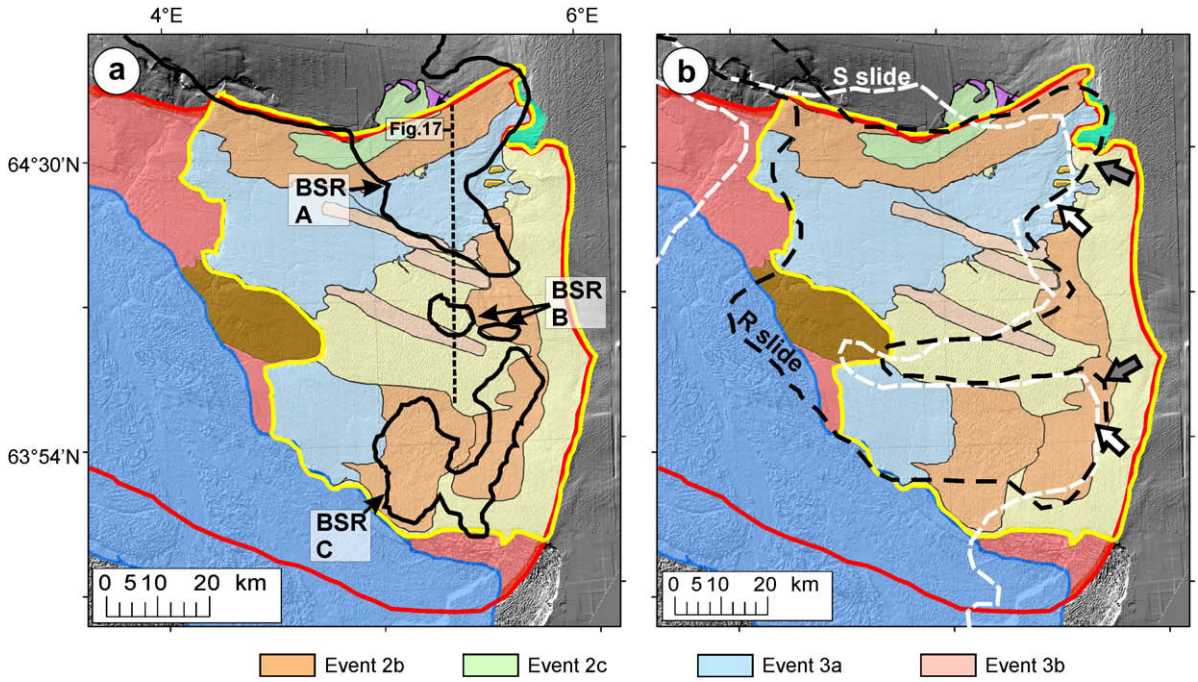


**Fig. 16.** Overlay of (a) the gas hydrate BSR and (b) the R and S palaeoslides on the slide development map in Fig. 15b. The grey and white arrows in (b) indicate the location of the headwall of the R Slide and S Slide, respectively. (The BSR and palaeoslides' boundaries have been traced from Bünz et al. (2003) and Solheim et al. (2005), respectively.)

The dissolution or dissociation of gas hydrates, due to changes in the pressure–temperature conditions, result in the release of a mixture of water and dissolved gas, or of free gas/water mixture, into the pore space, respectively (Sultan, 2007). Both of these transformations decrease the shear strength of the sediment, creating weak layers in the sub-seabed that are prone to failure (McIver, 1982; Nixon and Grozic, 2006). As a result, gas hydrate dissolution/dissociation may control the occurrence and locations of submarine slope instability. Gas hydrate dissolution/dissociation has been proposed by numerous authors as a trigger of slope instability within the Storegga Slide (Bugge et al., 1987; Mienert et al., 1998; Vogt and Jung, 2002; Sultan et al., 2004a,b; Mienert et al., 2005; Bünz et al., 2005). The common conclusion of these studies is that gas hydrates dissolution/dissociation may be a secondary process that weakened sediments and that partly explains the position of the main headwall of the Storegga Slide. It seems not, however, to be the primary cause of the Storegga Slide (Mienert et al., 2005).

Within the study area we observe some coincidence between the location of the BSR and the locations of a number of mass movements. The majority of areas affected by events 2b, 2c and 3a fall within the boundaries of BSR A, B and C (Fig. 16a). The eastern limits of BSR A and C correspond to the upslope limits of events 2b and 3a. The location of the BSR in Fig. 17 also correlates well with events 2b and 3a. Where the BSR intersects the main headwall, the morphology of the latter is steep and irregular (Figs. 13, 16). Where there is no BSR, the main headwall consists of a very gentle and continuous break of slope. We therefore propose gas hydrate dissolution/dissociation as one of the geological factors that determined the extent and style of failure in events 2b, 2c and 3a. Gas hydrate dissolution/dissociation likely occurred in the Storegga region due to warming after the last deglaciation, and by the time the Storegga Slide took place $8100 \pm 250$ cal yr BP, the thermal signal would have reached the base of the gas hydrate stability zone (Vogt and Jung, 2002). In particular in the area between 400 and 800 m water depth, the gas hydrates would have dissolved/dissociated, releasing gas and water, increasing the pore pressure and destabilising the slope (Sultan et al., 2004b; Mienert et al., 2005; Nixon and Grozic, 2006). The pockmarks located upslope of events 2b, 2c and 3a can be interpreted as evidence of this overpressure (Fig. 14). Gas hydrate dissolution/dissociation may also have taken place due to a decrease in lithostatic pressure after the removal of the O1–O2 sediment sub-units during event 1a, and the breaking up and mobilisation of the O3 sediment sub-unit during event 2a. The removal of overburden would decrease the confining pressures, leading to additional dissolution/dissociation and overpressure (Berndt et al., 2004). An increase in pore pressure due to gas hydrate dissolution/dissociation would have decreased the shear strength of the sediment, possibly leading to higher displacement and remoulding of the spreading blocks in events 2b and 2c, and the formation of debris flows and turbidity currents of event 3a. These events would have mobilised and evacuated sediment downslope of the BSR outcrop. This scenario fits well into the development model proposed in Section 5.2.

### 5.3.2. *Depositional framework and sedimentology*

The second geological cause for the observed morphological heterogeneities is the spatial variation in physical properties of the failed sediments and the setting in which they were originally deposited. The S and R Slides predate the Storegga Slide (Fig. 16b); they are dated at ~0.5 Ma and ~0.3 Ma respectively, and they have evacuated sediment from the north-eastern part of the Storegga Slide scar (Solheim et al., 2005). Repeated failure in this area accounts for the basin-shaped seafloor in the north-eastern Storegga Slide (Fig. 3b). Events 2b, 2c and 3a fall within the extent of the S and R palaeoslides inside the study area, and the upslope limit of events 2b and 3a coincide with the headwalls of the palaeoslides (Fig. 16b). The north-eastern boundary of the R headwall coincides with that of the Storegga Slide, which confirms that the northern sidewall of the Storegga Slide scar was formed by an event older than the Holocene slide (Brown et al., 2006). This means that the direction of sediment mobilisation in the north-eastern Storegga Slide was controlled by a pre-existing structure. We suggest that the scars formed by the S and R palaeoslides have favoured the

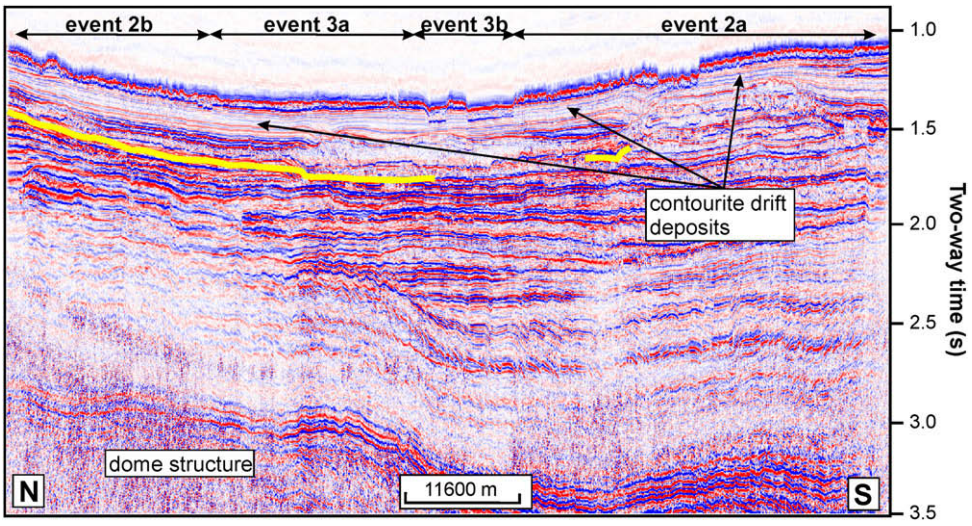


**Fig. 17.** Seismic dip profile across the north-eastern Storegga Slide (location shown in Fig. 16a). The thick yellow line indicates the gas hydrate BSR identified by Bünz et al. (2003) using seismic data of higher resolution than available for this study. Events 2a, 2b, 3a and 3b are all underlain by contourite drift deposits. However, only events 2b and 3a correlate well with the BSR underneath.

deposition of contourite drifts, transported northwards with the North Atlantic Current, from the North Sea Fan area (Bryn et al., 2005b). The deposition of contourite drifts is rapid, resulting in the build up of thick sediment bodies and the development of excess pore pressure in response to loading (Bryn et al., 2003). The contourite deposits are also characterised by high water content, low permeability and low density (Berg et al., 2005). Another important property of contourite drifts is their draping and smoothing of rough slide scars and glacial debris flow deposits, which facilitates the formation of extensive quasi-planar slip surfaces within the drift deposits. Because of all of these characteristics, the distribution of contourite drift deposits within the palaeoslide scars may have promoted instability and determined the extent of failure in events 2b, 2c and 3a.

Both the presence of gas and lithology changes may have controlled the nature and extent of failure in events 2b, 2c and 3a. Although we observe that all of the mass movements in events 2 and 3 occur within or above contourite drift deposits, only events 2b, 2c and 3a fail as highly displaced and remoulded spreading, debris flows and turbidity currents, whereas the remaining events predominantly involved spreading (Figs. 15–17). Only these three events coincide with the presence of a gas hydrate BSR. This correlation would suggest that the presence of gas, possibly as a result of gas hydrate dissolution/dissociation, has played a role in determining the failure style. However, our geophysical database is not dense enough close to the headwall to rule out that lithology changes, such as the presence of debris flows, may have played a role in the style of failure further upslope and overprinted the processes where we have full data coverage.

## 6. Conclusions

The north-eastern Storegga Slide has been shaped by a variety of submarine mass movements. These have been mapped in detail using morphometric attributes, geomorphometric mapping, ridge characterisation and ISODATA. We propose a revised development model for the north-eastern Storegga Slide consisting of four major events. The first event entailed the removal of the surface O1–O2 sediment sub-units by debris flows and turbidity currents when the Storegga Slide was triggered. Loading by these sediments resulted in the formation of an evacuation structure in the distal part of the study area. Loss of support from this structure, reactivation of the S headwall and seismic loading triggered extensive spreading in the O3 sediment sub-unit up to the main headwall. In some areas, spreading blocks have undergone high displacement and remoulding. Parts of the spreading morphology and the underlying sediment sub-units elsewhere have been mobilised or removed by debris flows and turbidity currents. The renewed instability within the spreading areas is attributed to two geological factors: (i) gas hydrate dissolution/dissociation and pore pressure development due to post-glacial ocean warming, and a reduction in lithostatic pressure following the removal of the O1–O2 sediment sub-units in the first event, and possibly (ii) the preferential deposition of contourite drifts in pre-existing slide scars. A fourth event consisting of large, blocky debris flow caused localised compression and transpressive shearing in the southern part of the spreading area.

With respect to the development model proposed by Haflidason et al. (2004), our model replaces lobes 1 and 3 with nine mass movement events (events 1, 2 and 3). Apart from redefining the boundaries and stratigraphical order of some of the mass movements in Haflidason et al.'s (2004) model, we demonstrate that the development of the north-eastern Storegga Slide did not occur by simple retrogression of debris flows, and that a complex interaction of a variety of submarine mass movement types has shaped the seabed in this region. Among these mass movement types, spreading is shown to play a fundamental role across the entire study area. This type of mass movement had not been taken into consideration in previous development models of the Storegga Slide. Apart from introducing new types of geological processes such as sediment evacuation, debris sliding and compression, our development model attests to the extensive spatial continuity of submarine mass movements and their potential to evolve between different types. The model also demonstrates how the same sediment type can undergo failure in different ways, and that it is important to consider subsurface structures when investigating the development of large-scale slope instabilities.

## Acknowledgements

This research was supported by the HERMES project, EC contract no. GOCE-CT-2005-511234, funded by the European Commission's Sixth Framework Programme under the priority 'Sustainable Development, Global Change and Ecosystems'. We would like to

thank Norsk Hydro ASA for providing the bathymetric data and 2D seismic lines. BP Norway and the European North Atlantic Margin (ENAM) II Programme are acknowledged for making available the 3D seismic data set and TOBI sidescan sonar imagery, respectively. We are grateful to Stefan Bünz, University of Tromsø for providing the BSR depth data.

## References

Atakan, K., Ojeda, A., 2005. Stress transfer in the Storegga area, offshore mid-Norway. Marine and Petroleum Geology 22 (1–2), 161–170.

Berg, K., Solheim, A., Bryn, P., 2005. The Pleistocene to recent geological development of the Ormen Lange area. Marine and Petroleum Geology 22 (1–2), 45–56.

Berndt, C., Mienert, J., Vanneste, M., Bünz, S., 2004. Gas hydrate dissociation and seafloor collapse in the wake of the Storegga Slide, Norway. In: Wandås, B.T.G., Eide, E., Gradstein, F., Nystuen, J.P. (Eds.), Onshore–Offshore Relationships on the North Atlantic Margin. Norwegian Petroleum Society (NPF) Special Publication. Elsevier, Amsterdam, pp. 285–292.

Bouriak, S., Vanneste, M., Saoutkine, A., 2000. Inferred gas hydrates and clay diapirs near the Storegga Slide on the southern edge of the Vøring Plateau, offshore Norway. Marine Geology 163, 125–148.

Brown, H.E., Holbrook, W.S., Hornbach, M.J., Nealon, J., 2006. Slide structure and role of gas hydrate at the northern boundary of the Storegga slide, offshore Norway. Marine Geology 229, 179–186.

Bryn, P., Berg, K., Forberg, C.F., Solheim, A., Kvalstad, T.J., 2005a. Explaining the Storegga Slide. Marine and Petroleum Geology 22 (1–2), 11–19.

Bryn, P., Berg, K., Stoker, M.S., Haflidason, H., Solheim, A., 2005b. Contourites and their relevance for mass wasting along the Mid-Norwegian Margin. Marine and Petroleum Geology 22 (1–2), 85–96.

Bryn, P., Solheim, A., Berg, K., Lein, R., Forsberg, C.F., Haflidason, H., Ottesen, D., Rise, L., 2003. The Storegga Slide complex: repeated large scale sliding in response to climatic cyclicity. In: Locat, J., Mienert, J. (Eds.), Submarine Mass Movements and their Consequences. Kluwer Academic Publishers, The Netherlands, pp. 215–222.

Bugge, T., 1983. Submarine slides on the Norwegian continental margin with special emphasis on the Storegga area. Ph.D. thesis, Technical University, Trondheim.

Bugge, T., Befring, S., Belderson, R.H., Eidvin, T., Jansen, E., Kenyon, N.H., Holtedahl, H., Sejrup, H.P., 1987. A giant three-stage submarine slide off Norway. Geo-Marine Letters 7, 191–198.

Bungum, H., Lindholm, C., Faleide, J.I., 2005. Postglacial seismicity offshore mid-Norway with emphasis on spatio-temporal–magnitudal variations. Marine and Petroleum Geology 22, 137–148.

Bünz, S., Mienert, J., Berndt, C., 2003. Geological controls on the Storegga gas hydrate system of the mid-Norwegian continental margin. Earth and Planetary Science Letters 209, 291–307.

Bünz, S., Mienert, J., Bryn, P., Berg, K., 2005. Fluid flow impact on slope failure from 3D seismic data: a case study in the Storegga Slide. Basin Research 17 (1), 109–122.

De Blasio, F.V., Elverhøi, A., Issler, D., Harbitz, C.B., Bryn, P., Lien, R., 2004. Flow models of natural debris flows originating from overconsolidated clay materials. Marine Geology 213, 439–455.

De Blasio, F.V., Issler, D., Elverhøi, A., Harbitz, C.B., Ilstad, T., Bryn, P., Lien, R., Løholt, F., 2003. Dynamics, velocity and run-out of the Giant Storegga Slide. Geophysical Research Abstracts 5, 223–230.

Drăgut, L., Blaschke, T., 2006. Automated classification of landform elements using object-based image analysis. Geomorphology 81, 330–344.

Evans, I.S., 1990. General geomorphometry. In: Goudie, A.S., Anderson, M., Burt, T., Lewin, J., Richards, K., Whalley, B., Worsley, P. (Eds.), Geomorphological Techniques. Routeledge, London, pp. 44–56.

Gauer, P., Kvalstad, T.J., Forsberg, C.F., Bryn, P., Berg, K., 2005. The last phase of the Storegga Slide: simulation of retrogressive slide dynamics and comparison with slide-scar morphology. Marine and Petroleum Geology 22 (1–2), 171–178.

Haflidason, H., Lien, R., Sejrup, H.P., Forsberg, C.F., Bryn, P., 2005. The dating and morphometry of the Storegga Slide. Marine and Petroleum Geology 22 (1–2), 123–136.

Haflidason, H., Sejrup, H.P., Nygård, A., Bryn, P., Lien, R., Forsberg, C.F., Berg, K., Masson, D.G., 2004. The Storegga Slide: architecture, geometry and slide-development. Marine Geology 231, 201–234.

Judd, A.G., Hovland, M., 1992. The evidence of shallow gas in marine sediments. Continental Shelf Research 12, 1081–1095.

Kvalstad, T.J., Andersen, L., Forsberg, C.F., Berg, K., Bryn, P., Wangen, M., 2005. The Storegga slide: evaluation of triggering sources and slide mechanisms. Marine and Petroleum Geology 22 (1–2), 245–256.

Laberg, J.S., Vorren, T.O., Mienert, J., Evans, D., Lindberg, B., Ottesen, D., Kenyon, N.H., Henriksen, S., 2002. Late Quaternary palaeoenvironment and chronology in the Trænadjupet Slide area offshore Norway. Marine Geology 188, 35–60.

McIver, R.D., 1982. Role of naturally occurring gas hydrates in sediment transport. American Association of Petroleum Geologists Bulletin 66 (6), 789–792.

Micallef, A., Berndt, C., Masson, D.G., Stow, D.A.V., 2007a. Submarine spreading: dynamics and development. In: Lykousis, V., Sakellariou, D., Locat, J. (Eds.), Advances in Natural and Technological Hazards Research. Springer, Netherlands, pp. 119–128.

Micallef, A., Berndt, C., Masson, D.G., Stow, D.A.V., 2007b. A technique for the morphological characterization of submarine landscapes as exemplified by debris flows of the Storegga Slide. Journal of Geophysical Research 112, F02001.

Micallef, A., Masson, D.G., Berndt, C., Stow, D.A.V., 2007c. Morphology and mechanics of submarine spreading: A case study from the Storegga Slide. Journal of Geophysical Research 112, F03023.

Mienert, J., Posewang, J., Baumann, M., 1998. Gas hydrates along the northeastern Atlantic Margin; possible hydrate-bound margin instabilities and possible release of methane. In: Henriet, J.P., Mienert, J. (Eds.), Gas Hydrates: Relevance to World Margin Stability and Climate Change. Geological Society of London Special Publication, vol. 137, pp. 275–291.

Mienert, J., Vanneste, M., Bünz, S., Andreassen, K., Haflidason, H., Sejrup, H.P., 2005. Ocean warming and gas hydrate stability on the mid-Norwegian margin at the Storegga Slide. Marine and Petroleum Geology 22 (1–2), 233–244.

Mitchell, N.C., Clarke, J.E.H., 1994. Classification of seafloor geology using multibeam sonar data from the Scotian Shelf. Marine Geology 121, 143–160.

Mulder, R., Cochonat, P., 1996. Classification of offshore mass movements. Journal of Sedimentary Research 66 (1), 43–57.

Nixon, M.F., Grozic, J.L.H., 2006. A simple model for submarine slope stability analysis with gas hydrates. Norwegian Journal of Geology 86, 309–316.

Paull, C.K., Ussler, W., Dillon, W.P., 2000. Potential role of gas hydrate decomposition in generating submarine slope failures. In: Max, M.D. (Ed.), Natural Gas Hydrates in Oceanic and Permafrost Environments. Kluwer Academic Publishers, Netherlands, pp. 149–156.

Riis, F., Berg, K., Cartwright, J., Eidvin, T., Hansch, K., 2005. Formation of large crater-like evacuation structures in ooze sediments in the Norwegian Sea. Marine and Petroleum Geology 22 (1–2), 257–273.

Rise, L., Ottensen, D., Berg, K., Lundin, E., 2005. Large-scale development of the mid-Norwegian margin during the last 3 million years. Marine and Petroleum Geology 22 (1–2), 33–44.

Sloan, E.D., 1998. Physical/chemical properties of gas hydrates and their application to world margin instability and climatic change. In: Henriet, J.P., Mienert, J. (Eds.), Gas Hydrates: Relevance to World Margin Stability and Climate Change. Geological Society Special Publication, vol. 137, p. 20.

Solheim, A., Berg, K., Forsberg, C.F., Bryn, P., 2005. The Storegga Slide complex: repetitive large scale sliding with similar cause and development. Marine and Petroleum Geology 22 (1–2), 97–107.

Sultan, N., 2007. Excess pore pressure and slope failures resulting from gas-hyrdates dissociation and dissolution. In: Offshore Technology Conference, Houston, Texas, p. 9.

Sultan, N., Cochonat, P., Canals, M., Cattaneo, A., Dennielou, B., Haflidason, H., Laberg, J.S., Long, D., Mienert, J., Trincardi, F., Urgeles, R., Vorren, T.O., Wilson, C., 2004a. Triggering mechanisms of slope instability processes and sediment failures on continental margins: a geotechnical approach. Marine Geology 213 (1–4), 291–321.

Sultan, N., Cochonat, P., Foucher, J.P., Mienert, J., 2004b. Effect of gas hydrates melting on seafloor slope instability. Marine Geology 213, 379–401.

Vogt, P.R., Jung, W.Y., 2002. Holocene mass wasting on upper non-Polar continental slopes – due to post-Glacial ocean warming and hydrate dissociation? Geophysical Research Letters 29 (9), 1341.